Thermochimica Acta 543 (2012) 211–217

Contents lists available at SciVerse ScienceDirect

Thermochimica Acta

journal homepage: www.elsevier.com/locate/tca

Determination of intrinsic kinetics parameters for MoO_3 chlorination with Cl_2 gas between 798 and 873 K

G. De Micco [a,b,c,*], M. Carignan [a], C.A. Canavesio [b], A.E. Bohé [a,b,d]

[a] Comisión Nacional de Energía Atómica (C.N.E.A.), Avenida Bustillo 9500, 8400 San Carlos de Bariloche, Argentina
[b] Consejo Nacional de Investigaciones Científicas y Técnicas (CONICET), Argentina
[c] Universidad Nacional de Cuyo, Instituto Balseiro, Avenida Bustillo 9500, 8400 San Carlos de Bariloche, Argentina
[d] Universidad Nacional del Comahue, Centro Regional Universitario Bariloche, 8400 San Carlos de Bariloche, Argentina

ARTICLE INFO

Article history:
Received 30 January 2012
Received in revised form 17 May 2012
Accepted 20 May 2012
Available online 29 May 2012

Keywords:
Chlorination
Molybdenum trioxide
Thermogravimtery
Intrinsic parameters

ABSTRACT

In this work the kinetics of the chlorination of molybdenum trioxide has been studied by thermogravimetry between 798 and 873 K. The starting temperature for the reaction of MoO_3 with chlorine is determined at about 770 K. The influence of gaseous flow rate, sample mass, temperature, and chlorine partial pressure in the reaction rate is analyzed for two MoO_3 samples having different particle size and morphology. The experimental conditions for chemical control of the reaction rate were established for both types of samples. An average activation energy of 211 kJ mol^{-1} and a reaction order of 1 with respect to chlorine partial pressure were determined for the chlorination of MoO_3 with gaseous chlorine. A complete rate equation was formulated that describes the reaction evolution of each type of solid.

1. Introduction

Chlorination reactions are applied in extractive metallurgy to produce valuable metals such as titanium and zirconium. Similarly, this process could be applied to low-grade mineral ores and complex residues where a certain valuable metal is combined with other elements in a multi-compound system, to extract the metal of interest [1,2].

Molybdenum compounds have a widespread variety of technological applications including hydroprocessing catalysts used in petroleum refineries, molybdenum-containing steel [3], polymer solar cells [4], Mo containing alloys for biomedical applications [5], among others, for this reason it is important to develop technological strategies to recover this metal from different types of wastes [6–9]. This is due not only to have economical sources of valuable metals but also from an environmental point of view. As an example, spent catalysts containing metals such as Mo, W and Ni are hazardous toxic wastes that need to be correctly treated. Chlorination is one of the possible ways of metal reclamation and, for that reason; studies on these reaction kinetics and mechanisms can be applied in the development of suitable recovery technologies.

The MoO_3 chlorination reaction has been investigated before by several authors. A literature review of the articles published on this subject until 1995 was presented by Djona et al. [10]. A variety of chlorinating agents were used in the works reviewed, such as Cl_2, $SOCl_2$, or CCl_4, PCl_5, or different Cl_2 mixtures: $Cl_2 + O_2 + N_2$, $Cl_2 + S_2Cl_2$. Most of the studies are devoted to the study of the carbochlorination reaction using different carbons, and others are conducted in the presence of additional solids such as soot. The literature review revealed that no systematic study about chlorination of MoO_3 by Cl_2 was reported. The work of Djona et al. [10] is a contribution on that subject. They determined a starting temperature of 873 K (600 °C), an activation energy of 165 kJ mol^{-1}, and a reaction order with respect to Cl_2 of 0.75 for the chlorination of MoO_3 with Cl_2–N_2. They determined the function that describes the solid evolution during the reaction $X = kt$ (reaction controlled by chemical reaction of grains having the form of slabs) [10]. Another work was published by Ojeda et al. [11] who studied the effect of working variables on the chlorination of MoO_3 in the presence of carbon black, they identified that the only reaction product was MoO_2Cl_2 by chemical analysis of the solid products. They performed a thermodynamic analysis based in ΔG° changes and concluded that formation of MoO_2Cl_2 is the most likely product for the chlorination of MoO_3. Guethert et al. [12] also determined that MoO_2Cl_2 is formed by the reaction of MoO_3 and chlorine (3.4% Cl_2–0.1% O_2–96.5% N_2), and in presence of moisture, hydrolysis of MoO_2Cl_2 leads to formation of MoO_3. Finally, the X-ray

* Corresponding author at: Comisión Nacional de Energía Atómica (C.N.E.A.), Avenida Bustillo 9500, 8400 San Carlos de Bariloche, Argentina.
E-mail address: demiccog@cab.cnea.gov.ar (G. De Micco).

0040-6031/$ – see front matter © 2012 Elsevier B.V. All rights reserved.
http://dx.doi.org/10.1016/j.tca.2012.05.026

List of symbols

A	superficial area of sample layer, m^2
D	gaseous diffusion coefficient for Ar–Cl_2 mixture, $m^2\ s^{-1}$
E	activation energy, kJ mol^{-1}
$g(X)$	solid reactant conversion function under the absence of the effect of interstitial diffusion, dimensionless
K	adsorption equilibrium constant of Langmuir adsorption isotherm, dimensionless
k^*	pre-exponential factor of the intrinsic reaction constant, s^{-1} kPa
k_{app}	apparent reaction rate constant, s^{-1}
$f(p_{Cl_2})$	rate dependence on Cl_2 partial pressure, kPa
n	particle shape factor in $g(X)$, dimensionless
N_{Cl_2}	flux of chlorine, mol $Cl_2\ s^{-1}\ m^{-2}$
$N_{Cl_2(exp)}$	experimental value of chlorine flux, mol $Cl_2\ s^{-1}\ m^{-2}$
$p_{Cl_2,s}$	partial pressure of chlorine at the surface of solid sample layer, kPa
$p_{Cl_2,b}$	partial pressure of chlorine in the bulk, kPa
R	gas constant, 8.314×10^3 kJ K^{-1} mol^{-1}
r_0	initial radius of the spherical or cylindrical particles, m
t	time, s
T	temperature, K
V_m	molar volume of the initial phase (MoO_3), $m^3\ mol^{-1}$
W_{MoO3}	molecular weight of MoO_3, g mol^{-1}
X	solid conversion, dimensionless
δ	boundary layer thickness, m
ϕ	Arrhenius pre-exponential factor, mol $m^{-2}\ s^{-1}$

diffraction pattern of MoO_2Cl_2 was reported for the first time in 2003 by Volkovicha et al. [13].

In this work the chlorination of molybdenum trioxide was studied. Two different reactive grade solids were measured to obtain the kinetic parameters of the reaction (activation energy and reaction order with respect to gaseous reactant). The results obtained can contribute to the study of the chlorination reaction of complex systems containing other species such as waste catalysts as well as for the design and development of molybdenum recovery processes involving chlorination.

2. Thermodynamical considerations

The phase stability diagram for Mo–O–Cl system including several molybdenum chlorides and oxychlorides was presented previously [12] and is not repeated here. For the reaction conditions used in our experiments (chlorine partial pressure 35 kPa used for chlorination reactions and oxygen partial pressure below 10^{-4} kPa) the stable solid state is MoO_2Cl_2 (at 773 K). Similarly, among all possible reactions between MoO_3 and Cl_2 the only one that has a negative ΔG° value (above 836 K) is the following:

$$MoO_3(s) + Cl_2(g) \rightarrow MoO_2Cl_2(g) + \frac{1}{2}O_2(g) \quad \Delta G^\circ \ \text{(kJ)} = -0.1268\ \ T(K) + 106.01 \tag{1}$$

Finally, equilibrium composition as a function of temperature was calculated with HSC software [14]. It was obtained that starting with chlorine and excess of molybdenum trioxide as input materials, the major gaseous products that will be formed are MoO_2Cl_2 and O_2 for temperatures between 798 and 873 K.

3. Experimental

The gases used in this work were Cl_2 of 99.8% purity (Indupa, Argentina) and Ar of 99.99% purity (AGA, Argentina). Two different MoO_3 were used for the study:

- MoO_3(I): Aldrich 99.99% trace metal basis. SIGMA ALDRICH Co. 3050 Spruce Street, St. Louis, MO 63103, USA.
- MoO_3(II): Alfa Aesar Puratonic 99.998% (metals basis), Johnson Matthey, 30 Bond Street, Ward Hill, MA 01835, USA.

The solids were well characterized by scanning electron microscopy (SEM 515, Philips Electronics Instruments), the morphology of each solid reactant is shown in Fig. 1. MoO_3(I) is formed by non-porous crystalline grains of 1–20 μm size, which form agglomerates of different sizes up to about 300 μm. MoO_3(II) is composed by needle shaped non-porous crystalline particles of about 200 μm length. In Fig. 1a and b the shape of the MoO_3(I) and (II) particles can be observed. In Fig. 1a (MoO_3(I)) several agglomerates of different sizes can be seen as separate particles, while in MoO_3(II) (Fig. 1b) no agglomerates are formed and each particle is a needle shaped grain itself. In Fig. 1c the surface of one agglomerate particle (MoO_3(I)) is shown in detail and in Fig. 1d the surface of a needle (MoO_3(II)) can be observed. According to SEM examinations, MoO_3(II) will have two types of pores: small pores formed among the spherical crystalline grains and large pores formed among agglomerates of different sizes, both of them in the range of macropores [15]. Meanwhile, MoO_3(II) will only have one type of pores formed among the needles, also in the range of macropores. BET areas [16] were measured with Kr for both type of samples, the values obtained were $1.2 \times 10^4 \pm 3 \times 10^2$ $cm^2\ g^{-1}$ and $1.64 \times 10^3 \pm 30$ $cm^2\ g^{-1}$ for the initial powders of MoO_3(I) and MoO_3(II) respectively. A theoretical calculation of the total surface area assuming spherical and cylindrical particles of average radius (5 and 25 μm) for MoO_3(I) and MoO_3(II) was made. The values obtained for both samples were about 3 orders of magnitude lower than the BET values, this is indicating that the solids have roughness or porosity which is below the SEM resolution (about 1 μm).

Isothermal and non-isothermal chlorination reactions were carried out in a thermogravimetric analyzer (TGA). This thermogravimetric analyzer consists of an electrobalance (Model 2000, Cahn Instruments, Inc.) suitable for working with corrosive atmospheres, a gas line and a data acquisition system. This experimental set-up has a sensitivity of ±5 μg while operating at 1223 K under a flow of 8 L h^{-1}. Samples of 0.5–20 mg were placed on a flat quartz crucible forming a loose packed bed, and inside the reactor an argon flow of 1.3 L h^{-1} was maintained. To begin the non-isothermal experiments, a chlorine flow of 0.8 L h^{-1} was introduced and, at the same time, the heating started with a ramp of 260 K h^{-1}.

For the isothermal runs, samples of MoO_3(I) and (II) powders were heated at the working temperature in flowing Ar for 1 h after which chlorine was injected into the reactor and mass change and time were simultaneously recorded. This procedure was employed to analyze the influence of gaseous flow rate, initial mass of the sample, temperature, and chlorine partial pressure on the reaction rate.

Partially chlorinated samples were analyzed by SEM and no morphological changes were observed, indicating that the overall reaction, which forms only gaseous products, largely takes place near the outer boundaries of the particles for both solids.

4. Results

4.1. Onset temperature of chlorination reaction

The starting temperature for the chlorination of MoO_3 was determined by non-isothermal thermogravimetric measurements.

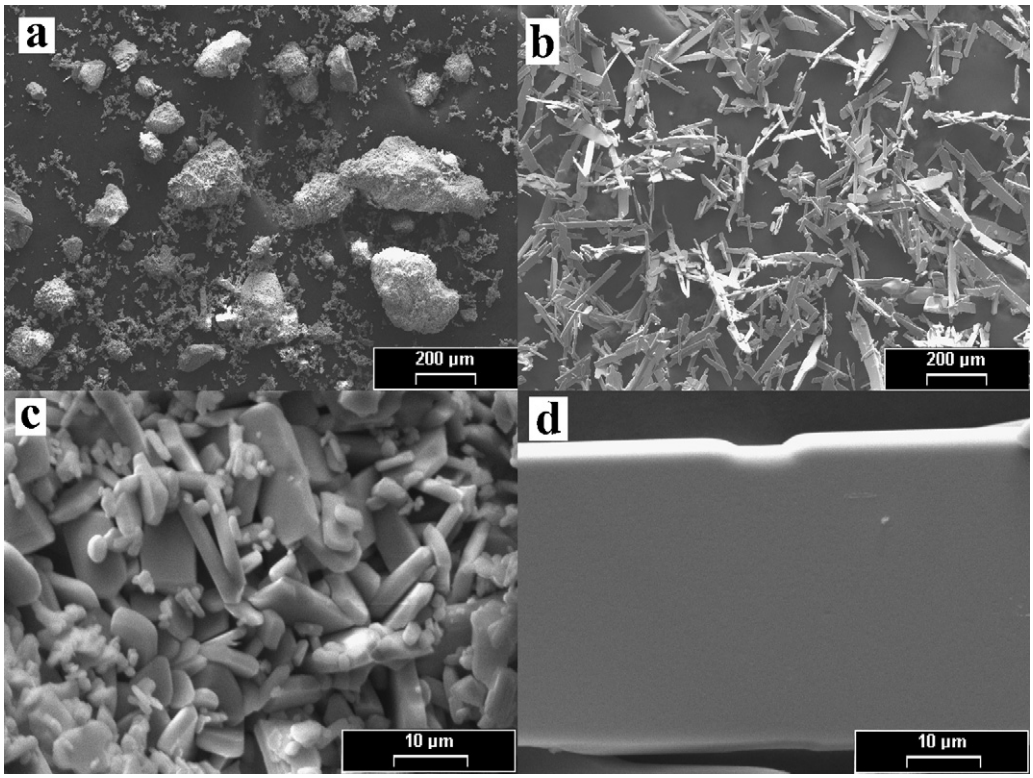

Fig. 1. SEM photographs of the initial sample (a) several agglomerates of different sizes of MoO_3(I), (b) particles of MoO_3(II), (c) the surface of an agglomerate of MoO_3(I), (d) the surface of a particle of MoO_3(II).

In Fig. 2 the ratio between the mass change and the initial mass of the sample as a function of temperature is shown for MoO_3 (I) and (II). The reaction starts at approximately 770 K, this value is 100 K lower than the previously reported [10]. The small difference between both curves is attributed to a higher value of specific surface area of MoO_3(I), which allows to detect the mass change for this sample slightly before the one corresponding to MoO_3(II). In both cases the sample starts to lose mass denoting the formation of a gaseous product. To identify the gaseous product, the reaction was carried out in a tubular reactor that allows to condense and collect the vapor species formed. The formation of MoO_2Cl_2 was determined by XRD (Fig. 3) and EDS. In the XRD pattern shown in Fig. 3, MoO_3 was also detected, this was attributed to the decomposition of MoO_2Cl_2 in presence of humidity [12].

The MoO_2Cl_2 has a high vapour pressure which indicates that it is formed as a vapor by the chlorination reaction, the vapor partial pressure of MoO_2Cl_2 is higher than 100 kPa at temperatures above about 500 K [14].

4.2. Determination of kinetic parameters

To determine the kinetic parameters it is first necessary to find the experimental conditions under which the reaction rate is not influenced by mass transfer processes (i.e. gaseous starvation, diffusion thorugh the gaseous boundary layer, diffusion throguh the sample pores).

Starvation occurs when a sufficient portion of the reactant is consumed by the solid, so that the particle is not in contact with a gas of bulk composition, but the gaseous reactant concentration

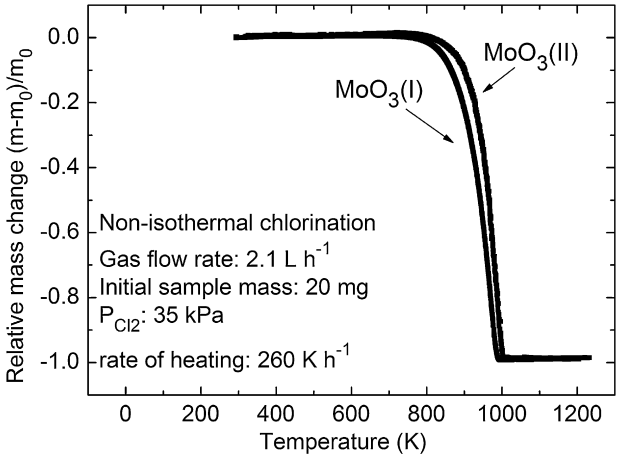

Fig. 2. TG curve for non-isothermal chlorination of MoO_3(I) and MoO_3(II).

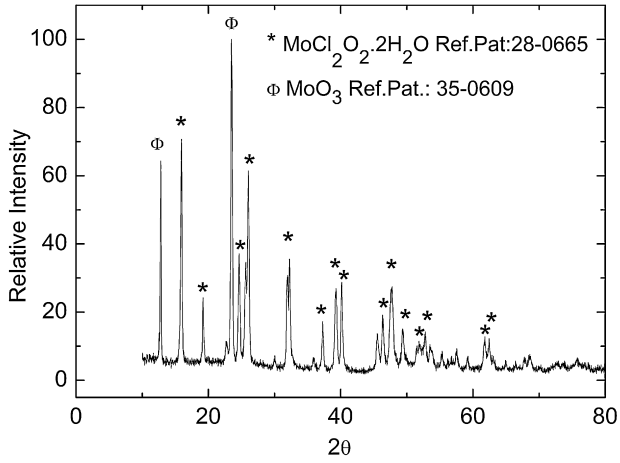

Fig. 3. XRD profile of the chlorination reaction product.

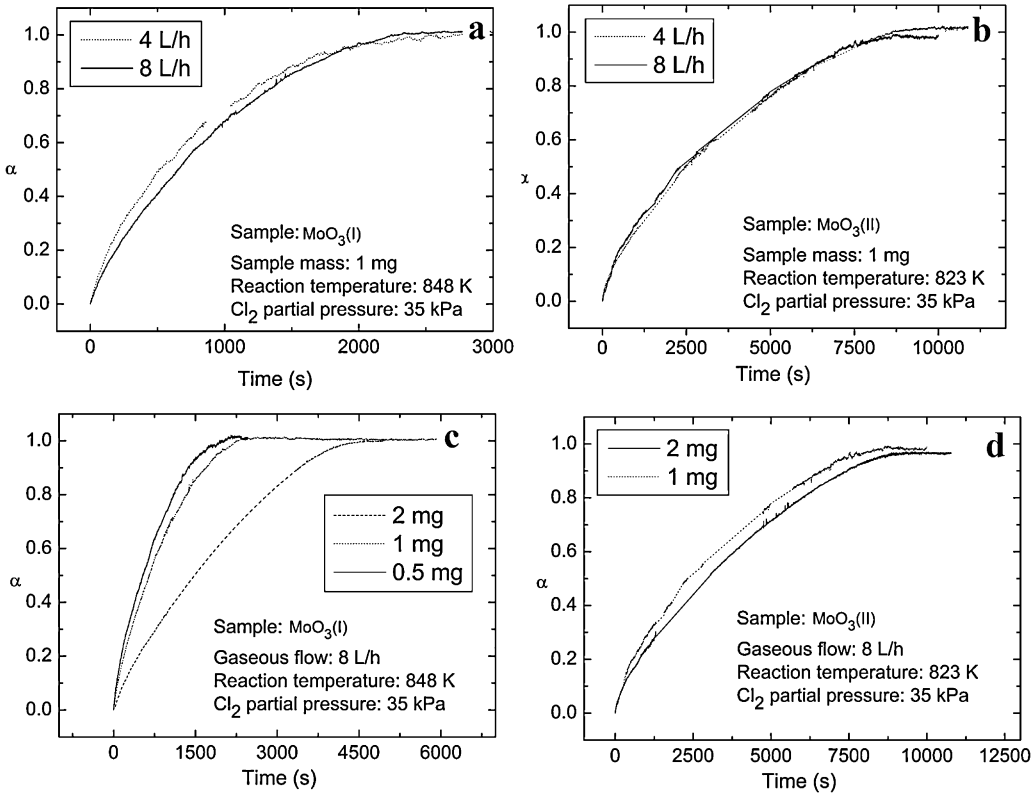

Fig. 4. Influence of gaseous flow rate in the chlorination of (a) MoO_3(I) and (b) MoO_3(II), and influence of sample mass in the chlorination of (c) MoO_3(I) and (d) MoO_3(II).

is less than this value [17,18]. In this condition, the driving force for the reaction will depend on the gas velocity, and an increase in the flow rate will cause the same increase in the reaction rate. The gaseous flow rate was raised from 4 L h^{-1} to 8 L h^{-1} in the chlorination of 1 mg of MoO_3(I) at 848 K and MoO_3(II) at 823 K to ensure that the systems were not in gaseous reactant starvation. The thermogravimetric (TG) curves obtained for the different flows are shown in Fig. 4 a and b. It can be seen that not increase in the reaction rate was obtained when duplicating the gaseous flow in both cases.

To analyze whether diffusion through the boundary layer affects the overall rate, isohermal chlorination experiments were perfomed for temperatures between 798 and 873 K and calculations were made to compare the experimental rate with the rate of chlorine diffusion between the top of the crucible and the top surface of the sample layer. The rate of diffusion through this space was estimated considering ordinary diffusion with the Fick's Law (Eq. (2)) the detalied description for the calculation of $p_{Cl_2,s}$, is explained elsewhere [19].

Table 1 shows the calculated and experimentally obtained molar fluxes of chlorine for MoO_3(I) and MoO_3 (II) samples. The values of D and p_{Cl_2} used in the calculation are also presented in the table.

$$N_{Cl_2} = -\frac{D}{RT\delta}(p_{Cl_2,s} - p_{Cl_2,b}) \quad (2)$$

The values of D were calculated for an Ar–Cl_2 mixture according to the Chapman-Enskog correlation [20] and the corresponding temperature, δ was considered to be the crucible heigth minus the sample thickness, and $p_{Cl_2,s}$ was calculated assuming equilibrium at the reaction surface.

The values of $N_{Cl_2(exp)}$ were calculated from the slope (r) of the mass changes vs. time curves corresponding to the TG measurments of the chlorination reactions at different temperatures. The slope was calculated by linear fitting these curves up to about 0.7 of conversion. According to the reaction stoichiometry and considering the reaction surface as the cross section area at the top of the sample layer, we have:

$$N_{Cl_2(exp)} = -r\frac{1}{W_{MoO_3}A} \quad (3)$$

For both samples it is seen that mass transfer controlled rate would be significantly faster than the observed rate. Consequently, we conclude that gas phase diffusion had no effect in the overall rate.

The effect of sample mass in the reaction rate was analyzed at 848 K for MoO_3(I) and at 823 K for MoO_3(II), as shown in Fig. 4c and d. For MoO_3(I) it can be seen that there is an increase in the rate of conversion as sample mass decreases from 2 to 1 mg, but further decrease of mass sample to 0.5 mg has no significant influence in the reaction rate (Fig. 4c), since the difference in the rate values obtained for 1 and 0.5 mg is within the range of the experimental scatter. The same happens for MoO_3(II) for sample masses of 2 and 1 mg (Fig. 4d).

For this reason, it can be concluded that for mass values lower than 1 mg the overall rate is controlled by intrinsic particle kinetics for both type of samples (MoO_3(I) and MoO_3(II)).

To determine the kinetic parameters, experiments were performed at different temperatures between 798 and 873 K with 35 kPa partial pressure of Cl_2 and 1 mg samples, for which the gaseous diffusion had no effect on the overall rate. Fig. 5 shows the TG curves obtained for different temperatures in terms of conversion vs. time.

The experimental conversion vs. time curves were fitted with a conversion function that describes a reaction proceeding according to a topochemically contracting geometry [17]. This equation may be used since the product of reaction being a gaseous species, the rate-determining step of the mechanism of reaction falls to be located at the surface of the reacting phase (i.e. the surface of the particles of MoO_3). Thus the kinetic curves may be described

Table 1
Comparison between rate of diffusion through crucible top and experimental rate of reaction.

Temperature [K]	$(p_{Cl_2})_{eq}$ [kPa]	D [m^2 s^{-1}]	Rate of diffusion between the top of the crucible and sample layer [mol Cl_2/(m^2 s)]	Experimental rate MoO_3(I) [mol Cl_2/(m^2 s)]	Experimental rate MoO_3(II) [mol Cl_2/(m^2 s)]
798	8.6	6.4E−05	6.6E−02	1.4E−05	5.7E−06
823	6.1	6.8E−05	7.5E−02	2.7E−05	2.1E−05
833	5.3	6.9E−05	7.7E−02	3.7E−05	–
848	4.2	7.2E−05	8.2E−02	7.1E−05	3.4E−05
873	3	7.6E−05	8.7E−02	–	9.4E−05

by the same rate law than that of a "topochemically contracting geometry":

$$g(X) = 1 - (1 - X)^{1/n} = k_{app}t \quad (4)$$

where X is the fractional conversion, and the value of n depends on the solid geometry.

If the hypothesis of variable separation holds, the apparent reacton constant (k_{app}) may be expressed by:

$$k_{app} = k^* e^{-E/RT} f(p_{Cl_2}) \quad (5)$$

where $f(p_{Cl_2})$ is a function of the reactant gas partial pressure and k^* an apparent pre-exponential factor.

This aproximation may not always be strictly valid. As an example, if the adsorption of chlorine at the surface of the particles is at equilibrium, and a subsequent step is rate-determining, the resulting dependence of k_{app} could be of the form:

$$k_{app} = k_0 e^{-E/RT} \frac{K\, p_{Cl_2}}{1 + K\, p_{Cl_2}} \quad (6)$$

where k_0 is the Arrhenius pre-exponential factor and K is the adsorption equilibrium constant of Langmuir adsorption isotherm, and is a function of temperature.

Our experimental results were well correlated with $n = 3$ for MoO_3(I) and $n = 2$ for MoO_3(II), as is shown in Fig. 6. With the values of k_{app} obtained at each temperature, the activation energy, E, can be obtained from the slope of the $\ln k_{app}$ vs $1/T$ plot, according to:

$$\ln k_{app} = -\frac{E}{RT} + \ln(k^* f(p_{Cl_2})) \quad (7)$$

This is shown in Fig. 7, where an activation energy of 216 ± 6 kJ mol^{-1} was calculated for MoO_3(I) and 207 ± 12 kJ mol^{-1} for MoO_3(II). This values are higher than the previously reported value of 165 kJ mol^{-1} for MoO_3 chlorination [10]. A possbile explanation for this difference is that in their work Djona et al. studied the effect of gas velocity on the reaction rate, and determined that it can be considered negligible beyond about 18 cm min^{-1} (or 30 L h^{-1}). They conclude that for values above that flow, starvation is eliminated and mass transfer effects are minimized. However, the effect of diffusion through sample pores may still be significant since they worked with large sample masses (100 mg). For this reason, the activation energy determined (165 kJ mol^{-1}) may correspond to a "mixed control regime" where diffusion within the pores limits the overall rate of reaction instead of a "chemical control regime" where the overall rate is controlled by the intrinsic chemical reaction.

To analyze the influence of p_{Cl_2}, experiments were conducted with different partial pressures of Cl_2 between 10 and 55 kPa, and with 1 mg samples at 823 K. The corresponding *conversion* vs. *time* curves were fitted according to Eq. (4) with $n = 3$ for MoO_3(I) and $n = 2$ for MoO_3(II). With the value of k_{app} obtained, the k_{app} vs. p_{Cl_2} plots were calculated (Fig. 8a and b). From this plots, a linear relation between k_{app} and p_{Cl_2} can be observed, which indicates that the reacion order with respect to partial pressure of chlorine is 1. Comparing this result with Eq. (6), the Langmuir model could still apply if $Kp_{Cl_2} \ll 1$ and K having a weak dependence on temperature. However, to make a thorough study on the adsorption mechanisim, much more experiments at different temperatures must be done, and that is beyond the scope of the present paper. In Fig. 8c and d the t_x (time requierd to achive a certain conversion value) vs. p_{Cl_2} plots for $x = 0.25$, 0.5 and 0.75 are presented, together with the fittings according to first order dependence on p_{Cl2}. The fitting equation is $t_x = C\, P_{Cl_2}^{-1}$, being $C = g(X(t_x))/(k^* e^{-E/RT})$, which is obtained combining and rearranging Eqs. (4) and (5) and calcualting $g(X)$ for the fix value of X corresponding to t_x. It can be seen that this function fits well the experimental data.

From Eq. (5), k^* for each temperature can be calculated substituting $f(p_{Cl_2})$ by p_{Cl_2}, ($p_{Cl_2} = 35$ kPa), and the activation energy previously obtained.

An average value of k^* was considered to establish the following relationship between conversion and time:

$$g(X) = 1 - (1 - X)^{1/3} = 1.91 \times 10^8 e^{-216/RT} p_{Cl_2} t \quad MoO_3(I) \quad (8)$$

$$g(X) = 1 - (1 - X)^{1/2} = 3.57 \times 10^7 e^{-207/RT} p_{Cl_2} t \quad MoO_3(II) \quad (9)$$

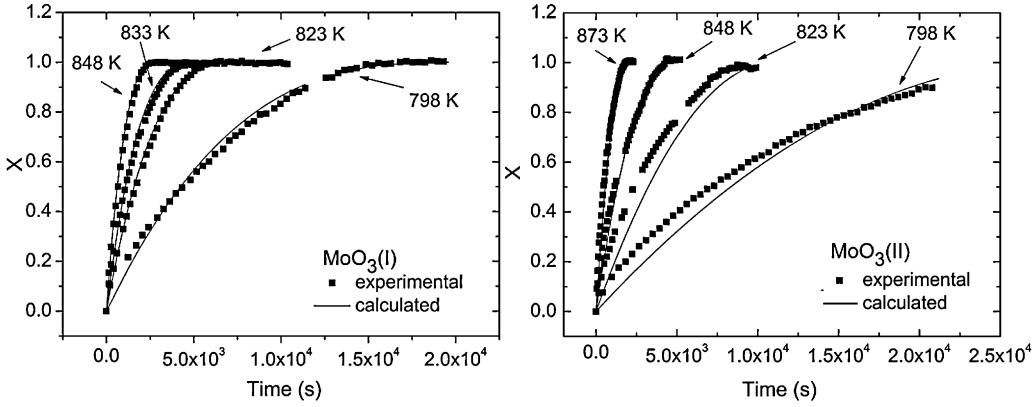

Fig. 5. Experimental conversion vs. time curves for temperatures between 798 and 873 K together with calculated conversion vs. time curves according to Eqs. (7) and (8).

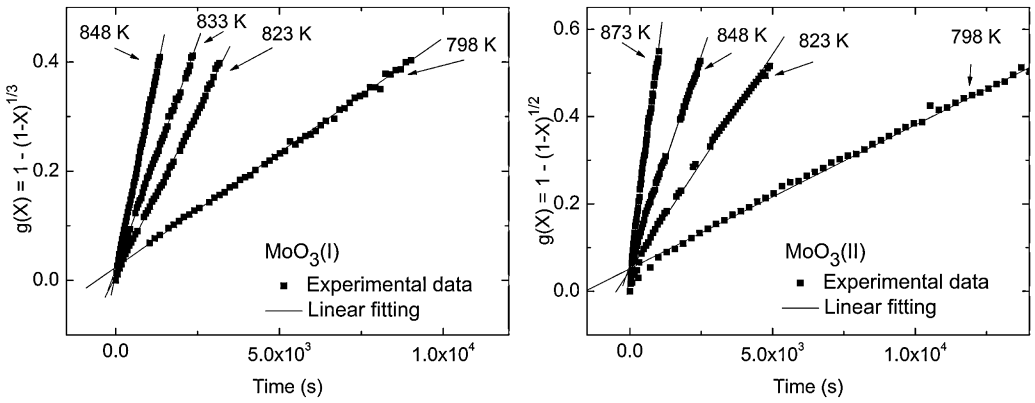

Fig. 6. (a, b) $g(X)$ vs. time plot for the chlorination of 1 mg of MoO_3(I) and MoO_3(II) at temperatures between 798 and 873 K, 35 kPa of chlorine partial pressure and gas flow rate of 4 L h^{-1}, linear fitting also shown.

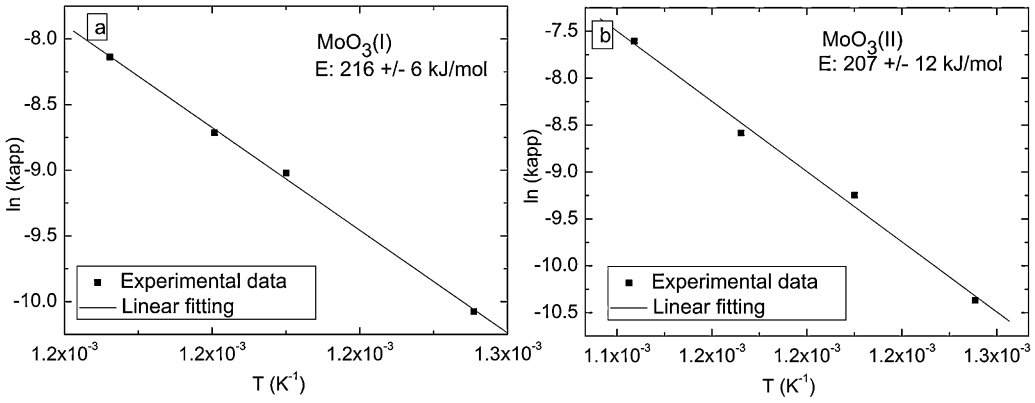

Fig. 7. $\ln k_{app}$ vs. T^{-1} plot for the calculation of activation energy (E): (a) MoO_3(I) and (b) MoO_3(II).

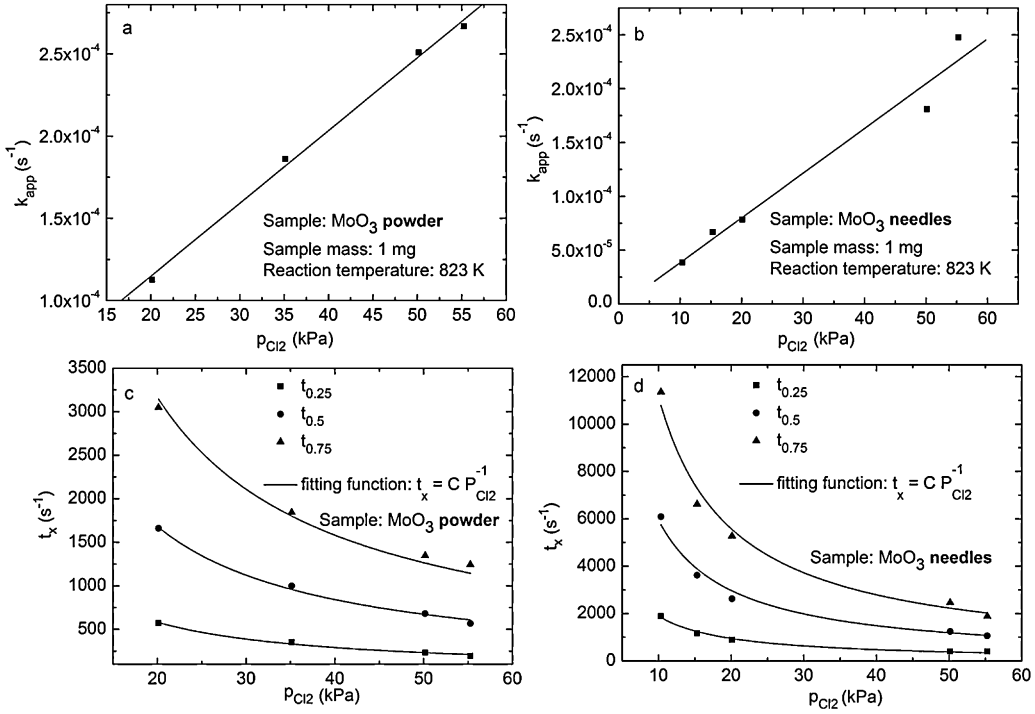

Fig. 8. (a, b) k_{app} vs. p_{Cl_2} plot for the determination of the reaction rate order with respect to p_{Cl_2} for MoO_3(I) and MoO_3(II). (c, d) Iso-conversional time vs. partial pressure of chlorine plot and fitting according to first order reaction with respect to p_{Cl_2}.

The corresponding conversion vs. time curves according to Eqs. (8) and (9) are plotted in Fig. 5 together with the experimental values. It shows that there is a good agreement between experimental and calculated conversions for all temperatures.

By differentiating Eqs. (8) and (9) with respect to time and rearrenging, the reaction rate expression can also be presented as:

$$\frac{dX}{dt} = 5.73 \times 10^8 e^{-216/RT} p_{Cl_2} (1-X)^{2/3} \quad MoO_3(I) \tag{10}$$

$$\frac{dX}{dt} = 7.14 \times 10^7 e^{-207/RT} p_{Cl_2} (1-X)^{1/2} \quad MoO_3(II) \tag{11}$$

It is noticed that, since the pre-exponentional factor is not an intrinsic value, the difference in the value obtained for each type of sample is due to the difference in morphology and particle size of the two sample types. According to the grain model [17] for chemical control of the reaction rate, and first order with respect of gaseous reactant, k^* can be expressed by:

$$k^* = \frac{V_m \phi}{r_0} \tag{12}$$

where ϕ is the Arrhenius pre-exponential factor of the reaction rate constant and does not depend of temperature and pressure conditions, r_0 is the initial radius of the spherical or cylindrical particles, and V_m is the molar volume of the initial phase (MoO_3).

The effect of particles size can be quantitativaly estimated from the y-intercept of the $\ln k_{app}$ vs $1/T$ plot, substituting k^* by Eq. (12) in Eq. (7). Accoding to SEM examination an average radius of 5 μm for MoO_3(I) and 27 μm for MoO_3(II) can be considered to calculate the value of ϕ ($V_m(MoO_3)$: 3.068×10^{-5} m^3 mol^{-1}). For both samples a value of 3.1×10^7 mol m^{-2} s^{-1} was obtained. Even though there is a good agreement between experimental results and theoretical considerations, the values of Arrhenius pre-exponentional factor (ϕ) is a rough calculation, since r_0 was estimated assuming spherical and cylindrical geometries of the reacting particles.

5. Conclusions

The rates of molybdenum oxide chlorination have been measured at temperatures between 798 and 873 K and chlorine partial pressures ranging from 10 to 55 kPa. The chlorination reaction started at 770 K, and the formation of MoO_2Cl_2 as predicted by thermodynamic considerations was confirmed by XRD.

For both type of samples used in this work (MoO_3(I) and (II)), the experimental conditions were achieved to measure the reaction rate under intrinsic kinetic rate controlled regime. The dependences of rate on gaseous reactant pressure, solid conversion and temperature were determined. Two intrinsic parameters were obtained: the activation energy of about 211 kJ mol^{-1} and the reaction order with respect to chlorine partial pressure of 1, while the Arrhenius pre-exponentional factor was estimated. Finally, a complete rate equation was formulated for each solid which differ in the pre-exponential factor and the solid evolution function due to the difference in morphology and particle size of the samples studied.

Acknowledgments

The authors would like to thanks the Agencia Nacional de Promoción Científica y Tecnológica (ANPCyT), Consejo Nacional de Investigaciones Científicas y Técnicas (CONICET) and Universidad Nacional del Comahue for the financial support of this work.

References

[1] B.G. Korshunov, Applications and potential uses of chlorination methods in metallurgy of non common metals, Metall. Rev. MMIJ 8 (2) (1992) 1–29, review.
[2] N. Kanari, E. Allain, R. Joussemet, J. Mochón, I. Ruiz-Bustinza, I. Gaballah, An overview study of chlorination reactions applied to the primary extraction and recycling of metals and to the synthesis of new reagents, Thermochim. Acta 495 (2009) 42–50.
[3] T.P. Hou, Y. Li, J.J. Zhang, K.M. Wu, Effect of magnetic field on the carbide precipitation during tempering of a molybdenum-containing steel, J. Magn. Magn. Mater. 324 (2012) 857–861.
[4] L. Shen, S. Ruan, W. Guo, F. Meng, W. Chen, Semitransparent inverted polymer solar cells using MoO_3/Ag/V_2O_5 as transparent anodes, Sol. Energy Mater. Sol. Cells 97 (2012) 59–63.
[5] C. Li, Y. Zhan, W. Jiang, b-Type Ti–Mo–Si ternary alloys designed for biomedical applications, Mater. Des. 34 (2012) 479–482.
[6] B.W. Jong, S.C. Rhoads, A.M. Stubbs, T.R. Stoelting: Report of Investigations 9252—United States, Bureau of Mines, Moscow, ID, 1989, pp. 1–27.
[7] Z. Li, C.Y. Cheng, A literature review of the recovery of molybdenum and vanadium from spent hydrodesulphurisation catalysts Part I.Metallurgical processes, Hydrometallurgy 98 (2009) 1–9.
[8] M. Marafi, A. Stanislaus, Spent hydroprocessing catalyst management: areview Part II. Advances in metal recovery and safe disposal methods, Resour. Conserv. Recycl. 53 (2008) 1–26.
[9] B.B. Kar, B.V.R. Murthy, V.N. Misra, Extraction of molybdenum from spent catalyst by salt-roasting, Int. J. Miner. Process. 76 (2005) 143–147.
[10] M. Djona, E. Allain, I. Gaballah:, Kinetics of chlorination and carbochlorination of molybdenum trioxide, Metall. Mater. Trans. B 26B (1995) 703–710.
[11] M.W. Ojeda, J.B. Rivarola, O.D. Quiroga, Study on chlorination of molybdenum trioxide mixed with carbon black, Miner. Eng. 15 (2002) 585–591.
[12] A. Guethert, R. Muenze, B. Eichler, Contribution to the thermodynamics of molybdenum–oxygen–chlorine system, J. Radioanal. Chem. 62 (1–2) (1981) 91–101.
[13] V.A. Volkovicha, T.R. Griffiths, R.C. Thied, B. Lewin, Behavior of molybdenum in pyrochemical reprocessing: a spectroscopic study of the chlorination of molybdenum and its oxides in chloride melts, J. Nucl. Mater. 323 (2003) 93–100.
[14] HSC Chemistry software version 6.12, Outotec Research Oy, Pori, Finland, 1974–2007.
[15] F. Rouquerol, J. Rouquerol, K. Sing, Adsorption by Powders and Porous Solids, Academic Press, 1999.
[16] S. Brunaver, P.H. Emmete, E. Teller, Adsorption of gases in multimolecular layers, J. Am. Chem. Soc. 60 (1938) 309–319.
[17] J. Szekely, J.W. Evans, H.Y. Sohn:, Gas-Solid Reactions, Academic Press, New York, NY, 1976, pp. 232 and 115–117.
[18] A.W. Hills, The importance of convective mass transfer in the reduction of hematite, Metall. Trans. B 98B (1978) 121–128.
[19] G. De Micco, A.E. Bohé, H.Y. Sohn, Intrinsic kinetics of chlorination of WO_3 particles with Cl_2 gas between 973 K and 1223 K (700 °C and 950 °C), Metall. Mater. Trans. B 42 (2) (2011) 316–323.
[20] J.O. Hirschfelder, C.F. Curtiss, R.B. Bird:, Molecular Theory of Gases and Liquids, Wiley, New York, USA, 1956.